

Article

Monitoring of Land Subsidence and Analysis of Impact Factors in the Tianshan North Slope Urban Agglomeration

Xiaoqiang Yi, Lang Wang, Hui Ci *, Ran Wang , Hui Yang  and Zhaojin Yan 

School of Resources and Geosciences, China University of Mining and Technology, Xuzhou 221116, China; ts24010006a31tm@cumt.edu.cn (X.Y.)

* Correspondence: cihui@cumt.edu.cn

Abstract: As one of the 19 key regions for comprehensive land development in China, the Tianshan North Slope urban agglomeration is significant for China's urban development when calculating the land subsidence and analyzing the impact factors. This study focused on eight cities in the Tianshan North Slope urban agglomeration, calculating the land subsidence rate from 18 January 2018 to 12 April 2023 using Sentinel-1A data and analyzing the spatiotemporal patterns and impact factors of land subsidence. The results showed that (1) the average land subsidence rate is mainly distributed between -30 and 10 mm/a, and the maximum subsidence rate can reach -358 mm/a. Land uplift mainly occurs in Hutubi County and Manas County. (2) From the transition matrix, landscape pattern index, and Moran's I, the spatiotemporal patterns of the land subsidence rate are obvious, with a spatial positive correlation. During the monitoring period, each administration experienced varying degrees of land subsidence or uplift processes. (3) Using GeoDetector to perform quantitative analyses, it was found that the hydrological environment is significant to land subsidence, and human activities, such as road network density and nighttime lighting, contribute the least to land subsidence, suggesting that it is related to the arid climate of the study area. This paper aims to provide theoretical support for the stable development of and production activities in the study area. This approach not only offers technical support but also provides guidance for evaluating, monitoring, and the early warning of land subsidence in the region.



Academic Editor: Francesca Cigna

Received: 11 December 2024

Revised: 10 January 2025

Accepted: 17 January 2025

Published: 20 January 2025

Citation: Yi, X.; Wang, L.; Ci, H.; Wang, R.; Yang, H.; Yan, Z. Monitoring of Land Subsidence and Analysis of Impact Factors in the Tianshan North Slope Urban Agglomeration. *Land* **2025**, *14*, 202. <https://doi.org/10.3390/land14010202>

Copyright: © 2025 by the authors. Licensee MDPI, Basel, Switzerland. This article is an open access article distributed under the terms and conditions of the Creative Commons Attribution (CC BY) license (<https://creativecommons.org/licenses/by/4.0/>).

Keywords: Tianshan North Slope urban agglomeration; Sentinel-1A data; land subsidence; spatiotemporal patterns; impact factors

1. Introduction

Land subsidence refers to the vertical descent of the ground surface relative to a certain datum (usually sea level) caused by natural or anthropogenic factors. It is typically caused by the consolidation and compression of underground loose strata, resulting in a decrease in the elevation of the earth's surface. This hazard typically manifests over extended periods and is associated with a notable incidence in fatalities and substantial economic repercussions annually [1–3]. Land subsidence can lead to the formation of surface cracks and ground subsidence, damage infrastructure, disrupt transportation networks, and pose severe risks to public safety and property [4,5]. It also presents significant challenges to sustainable urban development. At present, land subsidence of varying degrees has occurred in nearly 100 cities and regions across China, especially in the North China Plain [6], Fenwei Basin [7], Yangtze River Delta Plain [8], and other regions [9]. As time goes by, the degree and scope of land subsidence in these regions have expanded year by

year, bringing a serious impact on the local economy, society, and ecological environment. Ao et al. [1] found that most cities in China are facing a threat of land subsidence, which is caused by various factors such as excessive groundwater extraction, mining activities, building weight, and transportation infrastructure. Land subsidence can lead to changes in the flow of surface water and a decline in groundwater levels, which, in turn, can affect the growth of vegetation and the stability of ecosystems, exacerbating the ecological vulnerability of the Tianshan Mountains. Additionally, land subsidence can damage infrastructure such as roads, bridges, and buildings, posing threats to the safety of residents' lives and property, and affecting the normal operation and sustainable development of the city.

Traditional methods such as GPS and leveling are widely used in land monitoring due to their high precision, but they have limitations due to high costs, labor intensity, and the inability to cover large areas [10,11]. With the advancement of remote sensing technology, Synthetic Aperture Radar Interferometry (InSAR) [12,13] has gradually become an important method for monitoring land subsidence, landslides, volcanic activity, and the stability of infrastructure. Commonly used InSAR technologies include Differential Interference Radar (D-InSAR) [14], Small Baseline Subset InSAR (SBAS-InSAR) [15], and Persistent Scatterer InSAR (PS-InSAR) [16]. Compared to conventional methods, it boasts benefits such as continuous operation regardless of weather conditions, the capacity to see through cloud cover, extensive surveillance area, and reduced financial expenditure. These features make it particularly adept at conducting sequential surveillance of land subsidence. D-InSAR technology can accurately reveal the location and extent of ground subsidence, suitable for small-scale areas and short-term deformation monitoring; PS-InSAR technology has a millimeter-level monitoring precision, making it capable of detecting stable ground scatterers; SBAS-InSAR technology can perform deformation monitoring over large areas and provide high-quality deformation measurement results.

During the past decade, the utilization of InSAR technology for broad-scale delineation of geological hazards has seen considerable growth. The technique has become a key asset in the detection and surveillance of a wide array of geological risks [17]. By integrating InSAR technology with other data sources, we can not only identify ground subsidence but also analyze the impact of natural conditions or human activities (such as mining operations, geological activities, groundwater extraction, and building loads) on ground subsidence. Devara et al. employed DInSAR technology, along with data from Sentinel-1A and 1B, to successfully identify significant landslides in the Kodagu district of Karnataka, India. They found that after an earthquake, the rate of surface subsidence in the mineral development area was relatively high [18]. Teixeira et al. applied an upgraded QPS-InSAR technique to scrutinize the ground deformations resulting from mining activities [19]. Vaka et al. used multiple ascending and descending pass C-band Sentinel-1 images to study an earthquake's pre- and post-seismic surface displacements [20]. He et al. employed both PS-InSAR and SBAS-InSAR methodologies to analyze surface deformation and associated time series data. They found that geological structure, groundwater extraction, reclamation, and engineering construction all have impacts on land subsidence. The land subsidence of fault belts and seismic focus areas was significant, and the area above the clay layer settled significantly [21]. Compared to D-InSAR and PS-InSAR technology, SBAS-InSAR technology leverages the coherence of spatial distribution, exhibiting higher coherence. This technique has a relatively lower requirement for the amount of data in the time series because it does not rely on a single pixel point but instead utilizes the coherence of the spatial distribution. Moreover, SBAS-InSAR technology can make use of all available interferometric pairs, which enhances its practicality, especially when dealing with large-area ground deformation monitoring. Therefore, SBAS-InSAR technology is considered

more effective and widely applicable in practical applications due to its flexibility in data utilization and processing, as well as its reduced requirements for coherence [22–24].

Positioned within the central region of the Silk Road Economic Belt, the Tianshan North Slope urban cluster (TSNSUA) has distinguished itself as the most flourishing economic area in Xinjiang and a key pillar within the Silk Road Economic Belt. It is anticipated to develop into the strategic nucleus for the expansion of urbanization in Xinjiang in the forthcoming period [25–27]. With the continuous influx of an employed population, the local economy has been significantly boosted. Nevertheless, this surge in population has also resulted in a boom in infrastructure development, an enlargement of transportation networks, and excessive extraction of groundwater, all of which add strain to the ground and heighten the likelihood of subsidence. Yet, the area has not established a sustainable system for monitoring subsidence, and there remains a deficit in understanding the phenomenon and its causes, which is inadequate for addressing the demands of urban growth and disaster management in the future.

Owing to the limited research conducted on land subsidence within TSNSUA, this study applied SBAS-InSAR technology, leveraging data from Sentinel-1A, to track and analyze the spatial and temporal patterns of land subsidence from 18 January 2018 to 12 April 2023. Additionally, by synthesizing information on the geological background and hydrologic environment, the study delved into the factors contributing to land subsidence. The objective of this study was to identify the origins of subsidence and furnish crucial data for urban operational safety and environmental conservation. It carries substantial theoretical and practical importance for disaster preparedness, alleviation, and surveillance, contributing to the enhancement of urban geological environment management and risk aversion proficiency.

2. Materials and Methods

2.1. Study Area

TSNSUA, with geographical coordinates ranging from 83°24' E to 91°56' E and 40°18' N to 46°11' N, encompasses areas including Urumqi City, Changji City, Shawan County, Wujiaqu City, Shihezi City, Manas County, Fukang County, and Hutubi County (Figure 1) [28]. The terrain of the region spans the Tianshan Mountains, alluvial plains, and the Gurbantunggut Desert, with an overall south-high–north-low topography. The elevation in most areas of the north is approximately 170 m, while in the south, due to the presence of the Tianshan Mountains, the highest elevation exceeds 5000 m. The region shows a distinct linear pattern, with cities primarily located along rivers and transportation arteries. For instance, cities such as Urumqi and Changji extend along the river valleys and transportation routes at the northern foot of the Tianshan Mountains, forming a linear urban belt along the river valleys and transportation lines. The area is located at the northern foot of the Tianshan Mountains, where the geological structure is complex, with developed faults and folds. These geological structures not only affect the location selection and layout of cities but also impose constraints on urban infrastructure construction and resource development. Due to the complex geological structure, geological disasters such as earthquakes, landslides, and mudslides occur from time to time, posing a serious threat to the economic development of the urban agglomeration and the safety of people's lives and property.

The total area of TSNSUA is approximately 215,400 km², accounting for 13% of the total area of Xinjiang, and characterized by a continental climate. The predominant soil type in this area is gray desert soil, and at higher altitudes, brown calcareous soil and marsh soil are also found [29]. The TSNSUA region has a typical temperate continental climate, with cold winters and hot summers, and precipitation peaks in the summer,

while being relatively scarce in winter and spring. This climatic pattern leads to increased reliance on groundwater, and frequent extraction has caused a drop in the water table, thereby impacting ground subsidence. Additionally, the region's rich mineral resources and frequent mining activities have also negatively affected ground stability, exacerbating the problem of ground subsidence. In the economic development of Xinjiang, TSNSUA holds a significant position, with its secondary and tertiary industries occupying a larger share in the overall industries of the region. Moreover, agriculture, animal husbandry, and mineral resource extraction form the two main economic pillars of the area, with the extraction of resources such as coal, oil, and natural gas playing a crucial role in the region's economic development.

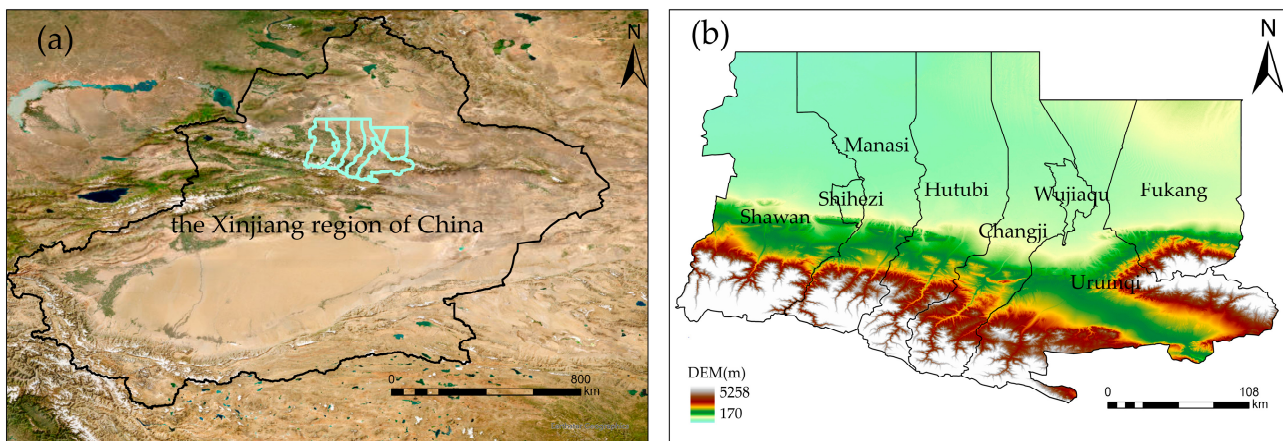


Figure 1. Study area: (a) the location of TSNSUA; (b) TSNSUA consisting of 8 cities.

TSNSUA has a sensitive ecological environment, valuable water resources, and abundant mineral resources. Surface deformation monitoring helps in the rational development and utilization of groundwater resources, prevents ground subsidence caused by overdevelopment, and protects biodiversity. It assists urban planners in better understanding the impact of urban development on geological structures, formulates more reasonable urban planning and land use policies, and maintains the sustainable development of the regional economy. Additionally, as TSNSUA is located at the border of multiple countries, surface subsidence monitoring is also an important part of transnational ecological protection and disaster management cooperation. Therefore, for TSNSUA, conducting surface subsidence monitoring is not only a technical issue but also a comprehensive issue involving the ecology, economy, and society, which is of great significance for ensuring the sustainable development of the region.

2.2. Data

Sentinel-1A, a radar satellite for earth observation, launched by the European Space Agency (ESA) in 2016, provides high-quality radar imaging data to users worldwide, offering vital support for all-weather, all-terrain monitoring. Utilizing C-band (3.75–7.50 cm) synthetic aperture radar imaging, it features all-weather conditions and a high resolution, making it capable of penetrating through clouds and fog for observations. The Sentinel series includes four imaging modes, with the wide-swath interferometric mode being suitable for land surface monitoring [30]. In this study, we utilized 132 Sentinel-1A single-look complex data (SLC) from 18 January 2018 to 12 April 2023 (<https://search.asf.alaska.edu/>, accessed on 20 July 2023) for monitoring ground subsidence in TSNSUA (Figure 2), with specific parameters detailed in Table 1. The Sentinel-1A SLC data are characterized by their high resolution. In this study, the Interferometric Wide (IW) imaging mode is employed, which offers a high resolution of 5 m by 20 m and covers a broad area of 250 km.

This allows the SAR images to precisely capture the fine details of the ground surface, providing valuable data for ground surface monitoring and analysis. Moreover, the selected SAR images fully cover the entire study area, and there is a significant overlap between adjacent image strips, with an overlap rate as high as 60%, thereby effectively ensuring the continuity and integrity of the data.

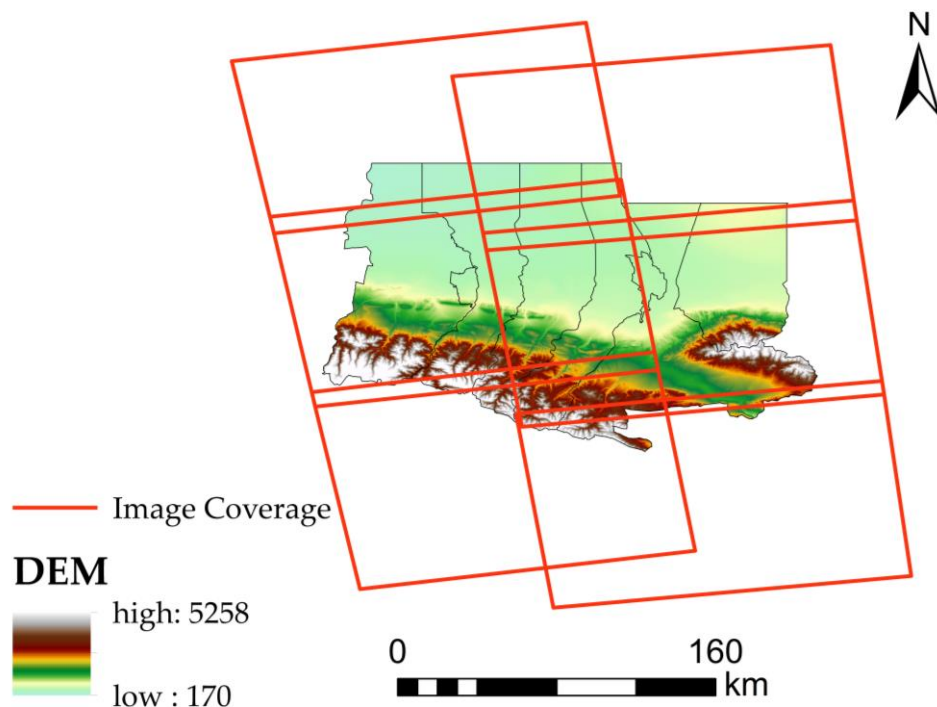


Figure 2. SAR image coverage.

Table 1. Specific parameters of SAR image.

Number of Orbital	Imaging Mode	Band	Resolution/m	Revisit Period/d	Polarization Mode	Selection Period/d
2 (Descend/Ascent)	IW	C	5 × 20	12	VV	90

Orbital data play a crucial role in InsAR data processing, exerting a key influence from the initial image co-registration to the final generation of deformation maps. The precise orbital files used in this paper are Precise Orbit Ephemerides (POD) data (<https://dataspace.copernicus.eu/>, accessed on 20 July 2023), aimed at achieving more accurate inversion results. These orbital data have a positioning accuracy of less than 5 cm, which is the highest level of precision for orbital data, and are typically available only 21 days after the acquisition of SAR data.

DEM data, serving as ancillary data, were derived from SRTM 30 m precision DEM data (<https://www.usgs.gov/>, accessed on 1 September 2023) to eliminate topographic effects from the interferograms using SBAS-InSAR technology. The algorithm for processing SRTM data to obtain a 30 m resolution DEM typically includes the following steps: data acquisition; data format conversion; data merging and clipping; no-data value filling; data smoothing and correction. Through these steps, SRTM data can be effectively processed into a 30 m resolution DEM, providing foundational data support for subsequent analysis.

Administrative division data of TSNSUA were downloaded from the National Catalogue Service for Geographic Information (<https://www.webmap.cn/>, accessed on 1 September 2023).

2.3. Method

The research process of this paper is shown in Figure 3.

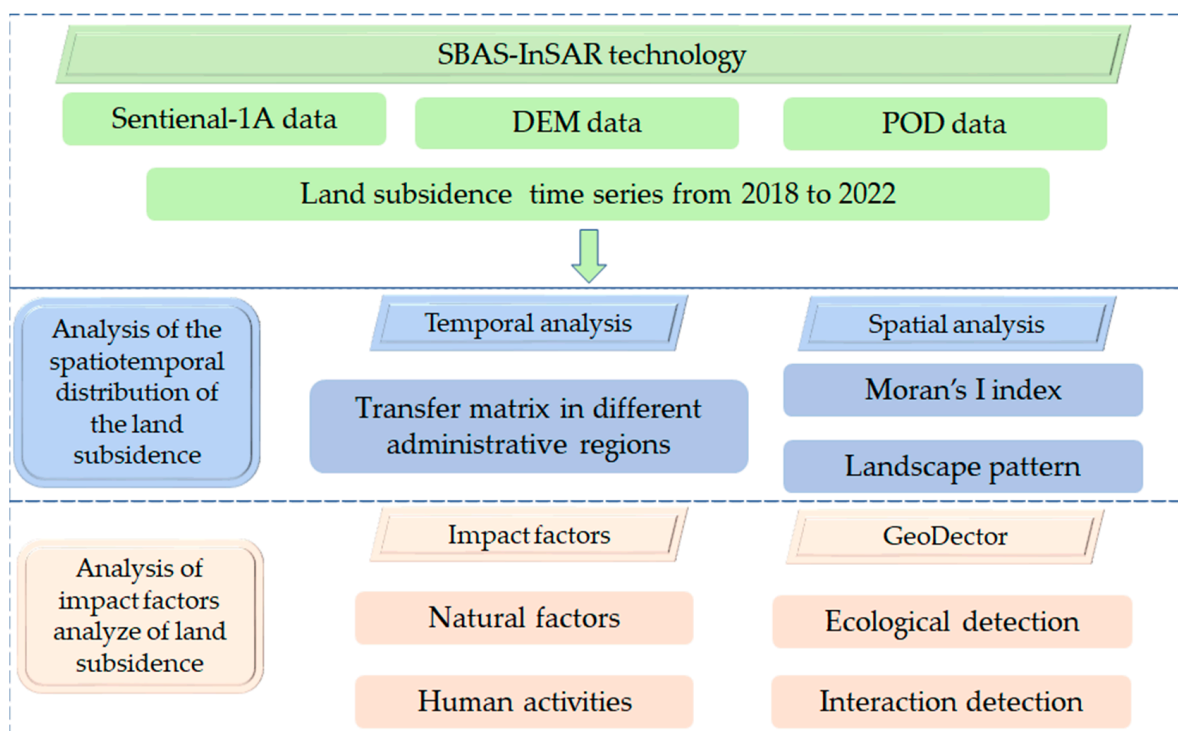


Figure 3. Study process.

2.3.1. InSAR Process

For SAR image, each pixel contains two parts of information: amplitude and phase, which can be represented by a complex number. A complex number consists of a real part and an imaginary part, with the real part corresponding to the amplitude value and the imaginary part corresponding to the phase value. Therefore, SAR is also referred to as SLC imagery. The value can be represented as formula [31]:

$$\varphi_{diff} = \varphi_{def} + \varphi_{top} + \varphi_{atm} + \varphi_{noise} \tag{1}$$

where φ_{def} reflects the phase shifts caused by surface deformation factors along the line of sight. φ_{top} reflects phase shifts caused by topographic factors. φ_{atm} reflects the atmospheric phase, which has a high degree of terrain auto-correlation, exists in the form of a low frequency, and can be suppressed by high-pass filtering methods. φ_{noise} reflects the noise phase, which exhibits random characteristics, exists in the form of a high frequency, and can be suppressed using low-pass filtering methods.

SBAS-InSAR technology, a derivation of time-series InSAR methodologies, focuses on extracting points with stable scattering properties from a lengthy series of SAR imagery. By establishing a network of these isolated, highly coherent points, SBAS-InSAR facilitates the accurate retrieval of surface deformation information [32].

In this study, we used ENVI/Scape5.6.2 for SBAS computation. The SBAS-InSAR technique integrates separate SAR images into multiple short-baseline sets by adhering to defined thresholds for vertical, temporal, and Doppler baselines. This approach helps to minimize the effects of perspective differences, thereby mitigating errors and the effects of decorrelation. In this paper, SBAS-InSAR is employed with temporal and spatial baselines as criteria, below a specific threshold, to combine all data into interferometric pairs. The

interferograms are created with a temporal baseline capped at 180 days and a spatial baseline limited to 45% [33] (Figure 4).

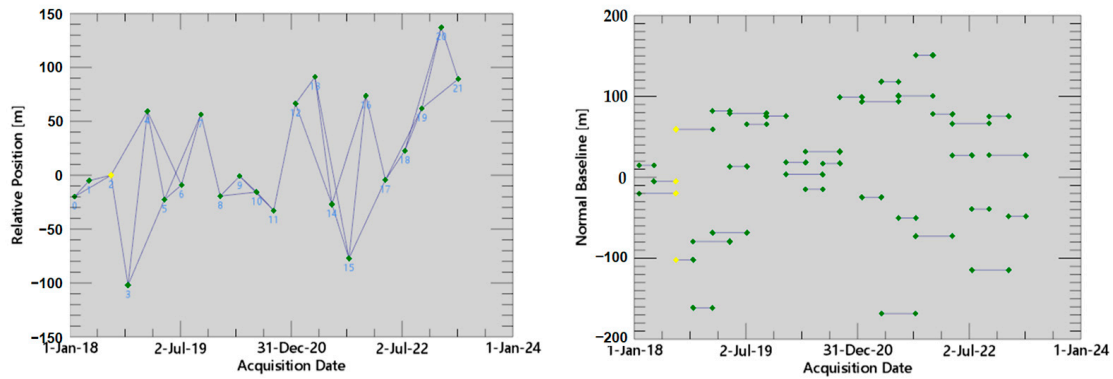


Figure 4. SBAS-InSAR partial image time baseline connection diagram. The lines represent the connection between the super master image and the slave image; the numbers represent the relative position relationship between images in different periods; the yellow dots represent the super master image, which is selected as the reference image in the processing process; the green dots represent the slave image, which is paired with the super master image or other images.

2.3.2. Transfer Matrix

In this paper, to conduct a more precise study and comparison of land subsidence phenomena across different regions, we employed a transition matrix and analyzed each city within TSNSUA based on administrative divisions, with a clear time frame set from 2018 to 2022, considering each year as a separate analysis period (2018–2019, 2019–2020, 2020–2021, 2021–2022). In this way, we can observe and analyze the trends of land subsidence during these periods, more accurately identify and compare the subsidence conditions of each city, and, thus, gain a deeper understanding of the dynamic processes and potential influencing factors of land subsidence. To make the presentation of the transition matrix more intuitive, we use a Sankey diagram to illustrate the transmission and variation of the land subsidence rate.

2.3.3. Spatial Autocorrelation Analysis

Ground subsidence generally exhibits spatial intercorrelation, and Moran's I index is a commonly used measure of spatial correlation [34]. It can reflect the similarity between ground subsidence and adjacent areas and is used to assess the scale and spatial positional relationships of ground subsidence levels within various regions of TSNSUA. The mathematical expression is as follows:

$$I = \frac{n}{S_0} \frac{\sum_{i=1}^n \sum_{j=1}^n w_{ij} z_i z_j}{\sum_{i=1}^n z_i^2} \quad (2)$$

$$S_0 = \sum_{i=1}^n \sum_{j=1}^n w_{ij} \quad (3)$$

$$z_i = \frac{I - E[I]}{\sqrt{V[I]}} \quad (4)$$

$$E[I] = -1/(N - 1) \quad (5)$$

$$V[I] = E[I^2] - E[I]^2 \quad (6)$$

where z_i is the deviation between the attributes of element i and its average value $x_i - \bar{X}$; w_{ij} is the spatial weight between elements i and j ; n equals the total number of elements;

and S_0 is the set of all spatial weights. The value range of I is $[-1, 1]$, $I > 0$ indicates that the variables have a positive correlation, $I < 0$ indicates a negative correlation, and $I = 0$ indicates no correlation.

2.3.4. Landscape Pattern Analysis

In this paper, incorporating ground subsidence velocities into the analysis of landscape patterns allows for the representation of variations in the configuration of ground subsidence across the terrain. We employed a set of five criteria to examine the spatial patterns of land subsidence within TSNSUA, including perimeter fractal dimension (PFD), max fractal dimension (MFD), Shannon's diversity index (SHDI), aggregation index (AI), and patch density (PD). Specifically, this study uses perimeter fractal dimension (PFD) to quantitatively describe the shape characteristics and complexity of ground subsidence patches of different severity levels. PFD can, to an extent, indicate the level of human activity interference, with a value range of $[1, 2]$. The closer the value is to 1, the less the area is affected by human activities; conversely, the closer the value is to 2, the greater the interference from human activities. Shannon's diversity index (SHDI) and max fractal dimension (MFD) are employed to investigate their diversity and complexity, reflecting the heterogeneity of the landscape and the types of dominant patches. The Aggregation Index (AI) is utilized to characterize the spatial configuration of these patches, reflecting the degree of aggregation of ground subsidence. The patch density (PD) is calculated to quantify the fragmentation degree of ground subsidence patches across various severity levels [35].

2.3.5. GeoDetector

Wang et al. [36] proposed GeoDetector to detect spatial heterogeneity and key factors, and it has been adopted in quite a number of studies since then. GeoDetector has a factor detector, a risk detector, an interaction, and an ecological detector [37–39]. Factor detection can assess the extent to which a certain factor explains the spatial variability of an attribute. The explanatory power of the factor is measured by calculating the q value, with a larger q value indicating a stronger ability to explain the spatial distribution of the attribute. Risk zone detection is used to determine whether there are significant differences in the mean values of attributes between different regions, which is tested using the t -statistic. Interaction detection can identify the interactions between different factors, assessing whether the combined effect of these factors on the dependent variable is enhanced or weakened, and whether the influences of these factors are independent. Ecological detection can compare whether there are significant differences in the impact of different influencing factors on the spatial distribution of attribute values.

The spatial variation of a certain independent variable z and its degree of consistency are expressed by detecting to what extent a certain independent variable z explains the dependent variable y , which is expressed by the q value. The q values were obtained by substituting the y and x data into the GeoDetector software (Excel 2007) run, and its value range was $[0, 1]$, and the larger the value, the stronger the explanation of the dependent variable y by the independent variable factor z . The model is as follows:

$$q = 1 - \frac{\sum_{h=1}^L N_h \sigma_h^2}{N \sigma^2} = 1 - \frac{SSW}{SST} \quad (7)$$

$$SSW = \sum_{h=1}^L N_h \sigma_h^2, \quad SST = N \sigma^2 \quad (8)$$

where $h = 1, \dots, L$ is the classification of dependent variable y or independent variable z ; N_h and N are the number of cells in layer h and the whole area, respectively, and they are

the variance in layer h and the whole area, respectively; and SSW and SST are the sum of variance within the layer and the total variance in the whole area, respectively.

This study used GeoDetector to analyze land subsidence, which can explain the contribution of different influencing factors to land subsidence and identify interactions between various factors. It is capable of handling interactions among multiple factors and is suitable for large-scale spatial data analysis. Based on previous research [1,40–46], the characteristics of the study area, data availability, and data volume requirements, we selected 10 impact factors to quantitatively analyze the explanatory power of various influencing factors on land subsidence with specific parameters detailed in Table 2. It is known that land subsidence is closely related to natural factors and human activities. Natural factors include geological background, hydrological environment, and topographic features; human activities include urban development and ground load. Soil is the material basis for the development of land subsidence, and the risk of land subsidence varies among different types of rock formations. Differences in clay content can also affect soil moisture content and porosity. This study selected two factors, geological lithology and clay content, to characterize the impact of geological background. TSNSUA is located in the arid and semi-arid northwest region. Considering the availability of data, this study selected two factors, potential evapotranspiration and precipitation, to characterize the impact of the hydrological environment. Elevation can affect vegetation growth and groundwater recharge, and slope can affect the stability of the slope structure, thereby affecting the probability of land subsidence. This study selected two factors, elevation and slope, to characterize the impact of topographic features. Population density and nighttime light are important factors of urban development, which can reflect the degree of urban construction activities to a certain extent. At the same time, ground load such as building density and road network density can also have an impact on land subsidence. This study selected four factors, population density, nighttime lighting, building density, and road network density, to characterize the impact of human activities.

Table 2. Ten impact factors for GeoDetector.

Natural Factors/Human Activities	Characterization Factors	Impact Factors	Abbreviation
Natural factors	Geological background	Geological lithology	G1
		Clay content	G2
	Hydrological environment	Precipitation	W1
		Potential evapotranspiration	W2
	Topographic features	Elevation	T1
		Slope	T2
Human activities	Urban development	Population density	H1
		Road network density	H2
	Ground load	Building density	H3
		Nighttime lighting	H4

3. Results

3.1. Inversion Results of Land Subsidence Based on SBAS-InSAR

Based on SBAS-InSAR technology processing flow, the vertical land subsidence rate of TSNSUA during the monitoring period was obtained (Figure 4). The average land subsidence rate during the monitoring period is mainly concentrated between -30 and 10 mm/a, with a maximum subsidence rate of -358 mm/a and a maximum uplift rate of 342 mm/a. The areas with severe land subsidence in the research area are concentrated in Hutubi County and Manas County, while the areas with severe land uplift are concentrated

in Shawan County in the southwest. It is speculated to be related to active geological tectonic activity (Figure 5).

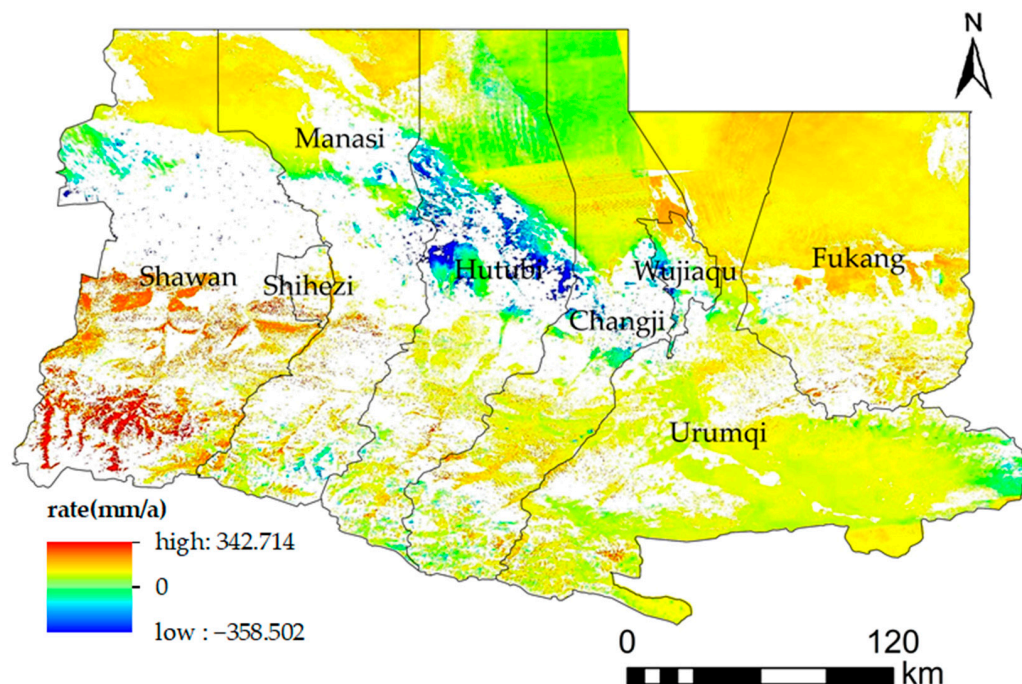


Figure 5. Land subsidence rate using SBAS-InSAR.

The SBAS-InSAR technique can provide high-precision, large-scale ground subsidence monitoring results by analyzing SAR images from multiple time phases. However, due to the inherent limitations of the SAR data and surface conditions, some errors and uncertainties may be introduced during the processing of SAR images with SBAS-InSAR. Field verification can provide more accurate ground subsidence data for calibrating and validating the accuracy of remotely sensed data, correcting potential errors, and ensuring the reliability of monitoring results. Moreover, on-site investigations help to understand the specific causes and mechanisms of ground subsidence, assisting governments in formulating more specific and accurate policies (Table 3).

Table 3. Field verification.





Number	Location	Description	Field Verification
1	Urumqi County	Land subsidence caused by excessive extraction of groundwater	
2	Hutubi County	Land subsidence caused by coal mining	

Table 3. Cont.

Number	Location	Description	Field Verification
3	Shawan County	Land subsidence caused by human activities such as quarrying	
4	Fukang County	Land subsidence caused by common soil erosion in the desert	

3.2. Analysis of Spatiotemporal Distribution Characteristics

In order to better assess the varying rates of land subsidence and subsequent spatial analysis, we divided the land subsidence rates into five subsidence levels based on the detailed classification criteria shown in Table 4. By precisely categorizing the rates of ground subsidence, we can gain a clearer understanding of the spatial distribution characteristics of subsidence. This facilitates the comparison of subsidence trends across different regions or time periods, providing crucial data support for studying the spatiotemporal variations in ground subsidence.

Table 4. The classification criteria of land subsidence rate.

Number	Subsidence Level	Subsidence Rate (mm/a)
1	Higher land subsidence rate zone	≤ -100
2	High land subsidence rate zone	$-100 \sim -50$
3	Middle land subsidence rate zone	$-50 \sim -20$
4	Low land subsidence rate zone	$-20 \sim 0$
5	Land uplift zone	>0

3.2.1. Transfer Matrix of Land Subsidence Rate

TSNSUA covers a vast area, and the natural economic conditions of each region are not entirely the same. Therefore, in order to better explore the temporal evolution characteristics of land subsidence, this section discusses and analyzes the land subsidence situation during the monitoring period at the scale of each administrative region (Figures 6–8).

In Urumqi City, the uplift area in 2018 was 7680 km² (91.6% of total area). In 2019, subsidence expanded to 33.7% of the area, with 2533 km² previously uplifted. By 2020, 97.2% of the area experienced subsidence, with 4580 km² showing high rates. In 2021, subsidence rates slowed, and 646 km² transitioned back to uplift. In 2022, 95.9% of the area was uplifted, including 7374 km² previously subsided.

In Changji City, the uplift area in 2018 was 3856 km² (89.8% of total area). In 2019, subsidence expanded to 65.3% of the area, with 2574 km² previously uplifted. By 2020, 98.6% of the area experienced subsidence, with 1032 km² showing increased high rates. In 2021, subsidence rates slowed, and 427 km² transitioned back to uplift. In 2022, 97.5% of the area was uplifted, including 3768 km² previously subsided.

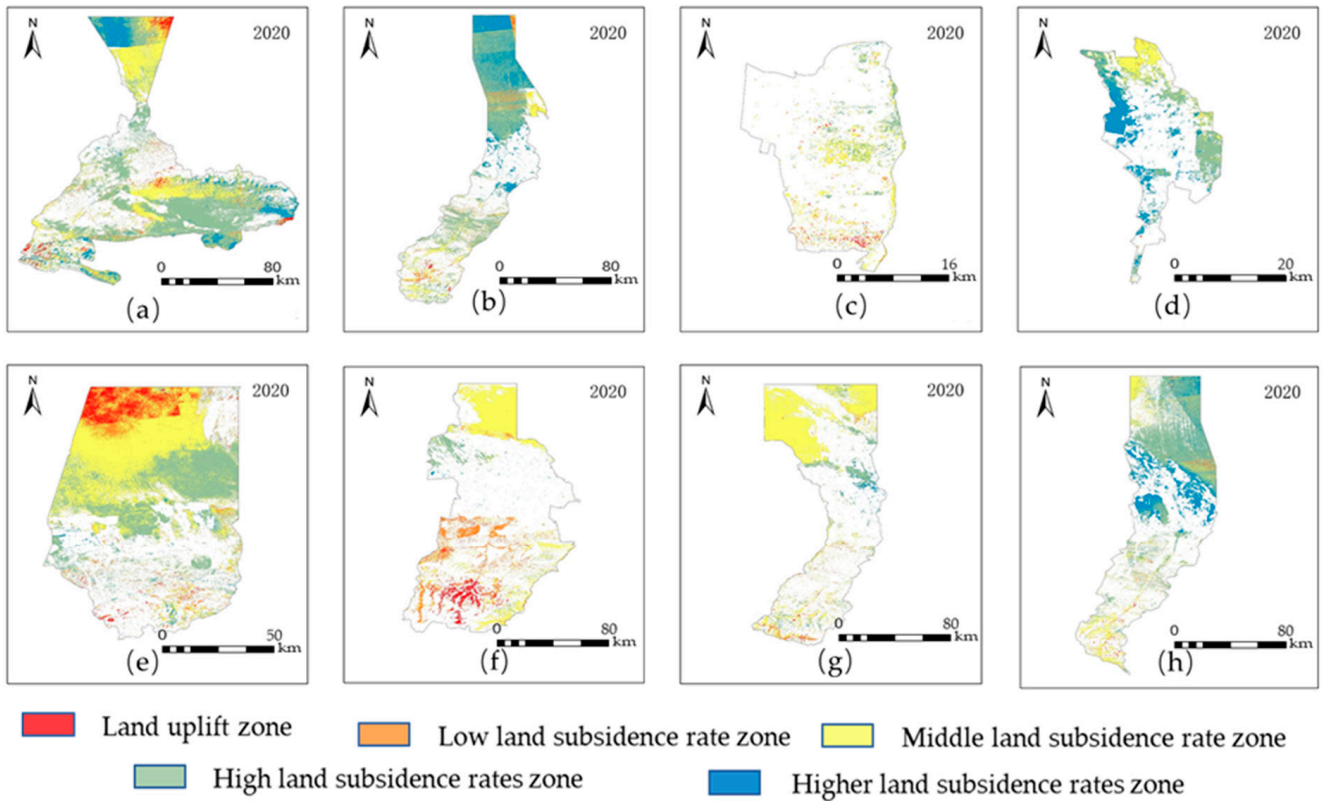


Figure 6. Subsidence levels of various administrative divisions in 2020. (a) Urumqi City; (b) Changji City; (c) Shihezi City; (d) Wujiaqu City; (e) Fukang City; (f) Shawan City; (g) Manas County; (h) Hutubi County.

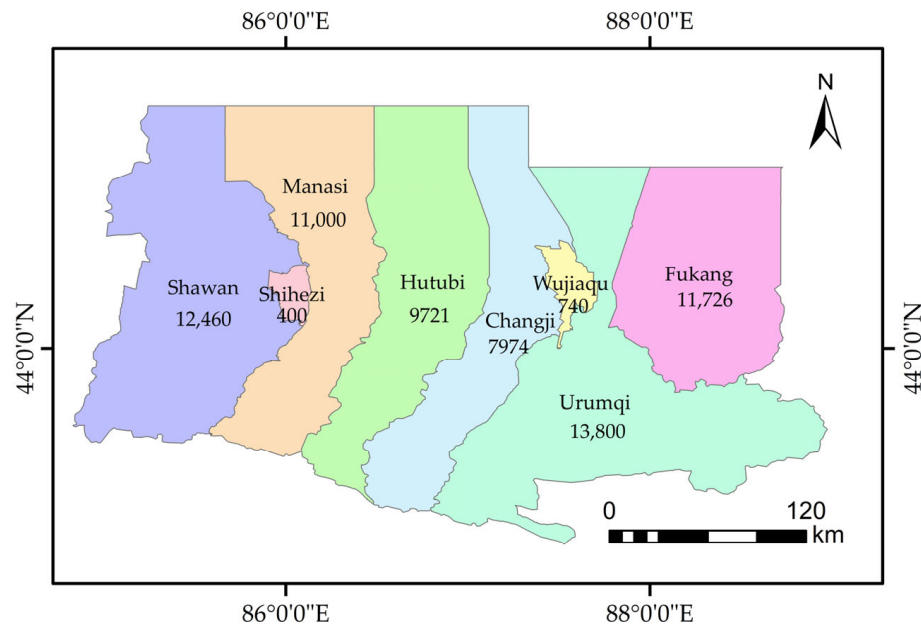


Figure 7. The boundary of each region. The numbers represent the area of each region in square kilometers.

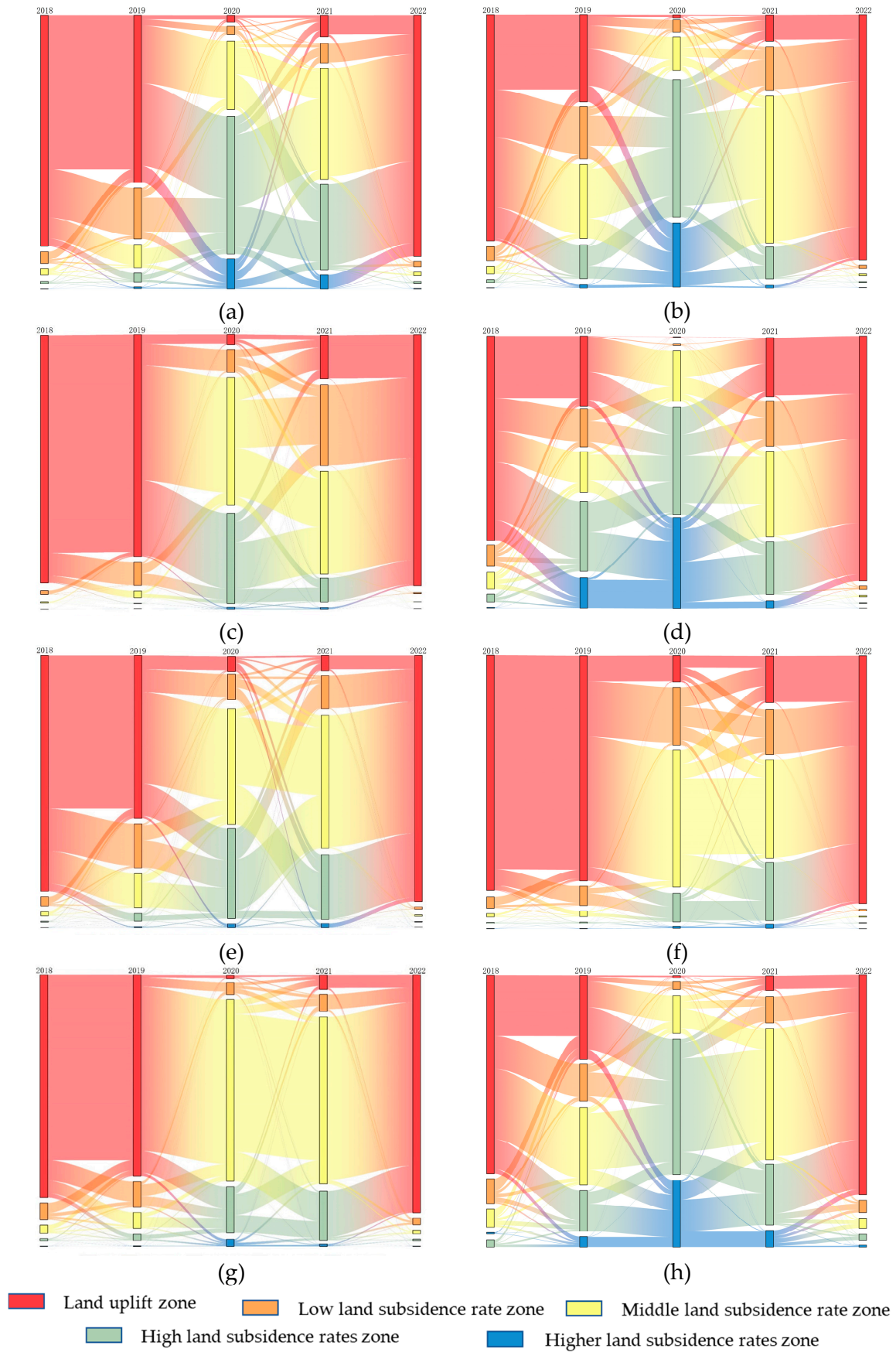


Figure 8. Transfer matrix of land subsidence at the scale of each administrative region. (a) Urumqi City; (b) Changji City; (c) Shihezi City; (d) Wujiaqu City; (e) Fukang City; (f) Shawan City; (g) Manas County; (h) Hutubi County.

In Shihezi City, there was no high-speed subsidence in 2018, with 56.36 km² uplifted (97.9% of total area). In 2019, subsidence expanded to 12.1% of the area, with 6.79 km² previously uplifted. By 2020, 96.1% of the area experienced subsidence, with significant increases in high- and middle-rate subsidence areas totaling 49.61 km². In 2021, subsidence rates slowed, and 8.89 km² transitioned back to uplift. In 2022, 99.3% of the area was uplifted, including 47.35 km² previously subsided.

In Wujiaqu City, the non-uplifted area in 2018 was 231.92 km² (81.4% of total area). In 2019, subsidence expanded to 72.1% of the area, with 161.47 km² previously uplifted. By 2020, 99.8% of the area experienced subsidence, with 103.49 km² showing high rates. In 2021, subsidence rates slowed, and 8.89 km² transitioned back to uplift. In 2022, 99.3% of the area was uplifted, including 65.48 km² previously subsided.

In Fukang City, the non-uplifted area in 2018 was 4578 km² (94.3% of total area). In 2019, subsidence expanded to 34.9% of the area, with 1467 km² previously uplifted. By 2020, 93.9% of the area experienced subsidence, with 2247 km² showing middle rates. In 2021, subsidence rates slowed in some areas, with 1471 km² transitioning from high to middle rates and 760 km² intensifying from middle to high rates. In 2022, 98.3% of the area was uplifted, including 4481 km² previously subsided.

In Shawan City, the uplift area in 2018 was 2873 km² (93.5% of total area). In 2019, subsidence slightly expanded, with 259 km² of previously uplifted area subsiding and 134 km² of previously subsided area stabilizing or uplifting. By 2020, 89.4% of the area experienced subsidence, with 1672 km² showing middle rates. In 2021, subsidence decreased, but 17 km² remained at high rates, 401 km² were at middle rates, and 223 km² intensified. In 2022, 98.5% of the area was uplifted, including 2464 km² previously subsided.

In Manas County, the non-uplifted area in 2018 was 2593 km² (89.1% of total area). In 2019, subsidence expanded to 19.5% of the area, with 436 km² previously uplifted. By 2020, 98.7% of the area experienced subsidence, with 2111 km² showing middle rates. In 2021, subsidence rates slowed in some areas, with 246 km² transitioning from high to middle rates and 334 km² intensifying from middle to high rates. In 2022, 95.2% of the area was uplifted, including 2624 km² previously subsided.

In Hutubi County, the non-uplifted area in 2018 was 3356 km² (79.2% of total area). In 2019, subsidence expanded to 66.7% of the area, with 2334 km² previously uplifted. By 2020, 99.1% of the area experienced subsidence, with 2297 km² showing high rates. In 2021, subsidence rates slowed, and 225 km² transitioned back to uplift. In 2022, 87.7% of the area was uplifted, including 3503 km² previously subsided.

For areas experiencing higher rates of ground subsidence, it is not advisable to continue with the construction of high-rise buildings, large structures, or transportation facilities with high precision requirements. Additionally, it is crucial to closely monitor changes in groundwater levels and strictly regulate the development of mineral resources and the extraction of groundwater in these areas. For areas with high subsidence rates, ground subsidence is likely to continue to worsen. In addition to focusing on monitoring, it is also necessary to actively take intervention measures, such as reducing the extraction of groundwater. For areas with middle subsidence rates, there is already a trend of ground subsidence. It is necessary to increase attention to these areas and impose restrictions on surface construction. For areas with low subsidence rates and regions where the ground is uplifting, there may be some fluctuations in the surface, but the subsidence is minimal or there is an uplift phenomenon, indicating that the ground is relatively stable. These areas are suitable for construction, but it is necessary to control the weight pressure of buildings. Industrial parks can consider relocating to these areas.

3.2.2. Spatial Autocorrelation Analysis of Land Subsidence Rate

A spatial autocorrelation analysis was conducted on the land subsidence rate of TSNSUA from 2018 to 2022. In this study, a grid scale of $1 \text{ km} \times 1 \text{ km}$ was used to analyze the spatial clustering characteristics of land subsidence in this study. The results showed that the Moran's I of the land subsidence rate was 0.74, which passed the significance test ($Z > 1.96, p < 0.05$), indicating a significant spatial positive correlation and a clear spatial agglomeration distribution feature during the monitoring period. This result indicates that the spatial distribution of land subsidence in the region exhibits a certain pattern of regular aggregation. For instance, subsidence is more pronounced in areas of coal mining or excessive groundwater extraction. Coal mining causes displacement and deformation of the strata, leading to surface subsidence. Additionally, excessive groundwater extraction results in a continuous decline in groundwater levels, forming a groundwater depression cone, which further exacerbates surface subsidence. Moreover, the presence of subsidence cones can affect subsidence in surrounding areas. The expansion of groundwater depression cones can cause a decline in groundwater levels in neighboring regions, leading to subsidence over a larger area. This spatial interaction results in a clear clustering pattern of subsidence in these areas.

3.2.3. Landscape Pattern Analysis of Land Subsidence Rate

Based on the Fragstats4.2 platform, the map of the land subsidence rate using SBAS-InSAR technology of TSNSUA was used as the data source to calculate the landscape pattern indices for different subsidence levels (Table 5).

Table 5. Landscape pattern indices of land subsidence rate.

Subsidence Level	PD	AI	PFD	MFD
Higher land subsidence rate zone	1.5006	24.6988	1.7190	0.0324
High land subsidence rate zone	5.8553	42.5601	1.5467	0.2913
Middle land subsidence rate zone	18.684	33.0502	1.6140	0.4531
Low land subsidence rate zone	41.664	71.5806	1.6082	17.383
Land uplift zone	44.400	54.5081	1.5990	6.6998

The analysis of the patch density (PD) calculation results shows that patches with a high land subsidence rate and a higher land uplift rate have lower fragmentation levels, while patches with a low land subsidence rate and land uplift rate are relatively fragmented. The analysis of the aggregation index (AI) calculation results shows that patches with a low land subsidence rate and land uplift have a higher degree of aggregation, while patches with higher land subsidence rates are relatively dispersed. The analysis of the perimeter fractal dimension (PFD) calculation results shows that the shape of patches with a higher land subsidence rate is relatively complex, with the largest perimeter area quantile, indicating that the higher subsidence area is most affected by human activities. During the monitoring period, the Shannon Diversity Index (SHDI) for land subsidence classification in TSNSUA was 0.8893, and the maximum patch area index (MFD) for a low subsidence rate and land uplift was 17.383 and 6.6998, respectively, which is much higher than other types. Therefore, it can be inferred that the land subsidence pattern in TSNSUA is dominated by a low subsidence rate and land uplift.

3.3. Analysis of Impact Factors

3.3.1. Contribution of Impact Factors to Land Subsidence

Based on using GeoDetector software (Excel 2007) to perform factor detection on 10 impact factors, the q-value was used to measure the explanatory power of each factor on

land subsidence during the statistical analysis of the results. Specifically, the increase in q -value indicates that the relevant variables have a stronger explanatory power and greater contribution to land subsidence phenomena. On the other hand, the p -value represents the probability of more extreme observational data occurring under the assumption of a zero hypothesis; a lower p -value indicates that the likelihood of the observed data being an extreme case is extremely low when the null hypothesis is true. The p -values for all factor detection results of the influencing factors are less than 0.001, suggesting that the test outcomes are highly unlikely to be the result of random variation and possess a high level of statistical significance; thus, these results can be deemed reliable and trustworthy (Figure 9).

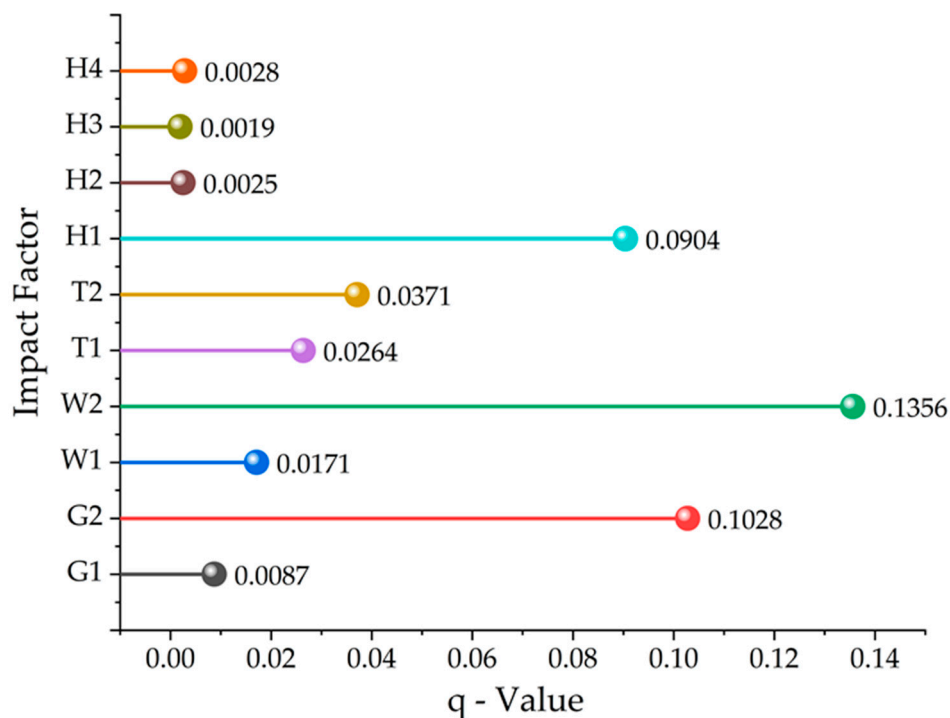


Figure 9. The contribution of impact factor.

The explanatory power of a single impact factor for different land subsidence varies, and the overall order is as follows: hydrological environment > geological background > human activities > topographic features. In reflecting urban land subsidence factors, groundwater changes have the strongest induction on land subsidence. In this paper, W1 and W2 directly affect groundwater content and soil moisture content, and they have the most significant effect on land subsidence in TSNSUA, where the q -values are 0.1356 and 0.0171, respectively, ranking the first and sixth, and their comprehensive explanatory power is significantly higher than other factors. Geological background provides a suitable environment for the occurrence of land subsidence. G2 and G1 affect the susceptibility of land subsidence, with q -values of 0.1028 and 0.0087, respectively, ranking the second and seventh. Human activities can affect urban water consumption and construction needs, indirectly affecting land subsidence. The q -values of H1, H4, H2, and H3 are 0.0904, 0.0028, 0.0025, and 0.0019. The topographic features affect the mobility of soil and groundwater, and they affect land subsidence to a certain extent. In this paper, the q -values of T2 and T1 are 0.0371 and 0.0264, respectively, ranking the fourth and fifth, with the lowest comprehensive explanatory power. The p -values of each individual impact factor are all below 0.001, indicating that extreme situations rarely occurred in this study, which indirectly demonstrates the reliability of the experimental results.

3.3.2. Ecological Detection and Factor Interaction Detection

Ecological detector is a method used to evaluate the differences in the influence of impact factors on land subsidence. When the q-values of two impact factors differ significantly, the ecological detector will record the result as Y, indicating the existence of a significant difference; on the contrary, if the difference is not significant, the result is denoted as N. Ecological exploration was conducted on the selected 10 impact factors G1, G2, H1, H2, H3, H4, W1, W2, T1, and T2.

Compared to other statistical methods, interaction detectors exhibit significant advantages in analyzing the interrelationships between variables. Its characteristic lies in the ability to identify existing interaction patterns by comparing the q-value of a single factor with the interaction q-value between factors. Unlike traditional statistical methods, interaction detectors are not based on the assumption of multiplication relationships and can detect interactions as long as they exist (Table 6 and Figure 10).

Table 6. The result of ecological detection.

Impact Factor	G1	G2	H1	H2	H3	H4	W1	W2	T1	T2
G1										
G2	Y (NE)									
H1	Y (NE)	N (NE)								
H2	N (NE)	Y (NE)	Y (NE)							
H3	N (NE)	Y (NE)	Y (NE)	N (NE)						
H4	N (NE)	Y (NE)	Y (NE)	N (BE)	N (NE)					
W1	N (NE)	Y (NE)	Y (NE)	N (NE)	Y (NE)	N (NE)				
W2	Y (NE)	Y (NE)	Y (BE)	Y (NE)	Y (NE)	Y (NE)	Y (NE)			
T1	Y (BE)	Y (NE)	Y (NE)	Y (NE)	Y (NE)	Y (NE)	N (BE)	Y (NE)		
T2	Y (BE)	Y (NE)	Y (NE)	Y (NE)	Y (NE)	Y (BE)	Y (BE)	Y (NE)	N (BE)	

NE reflects nonlinear enhancement effects; BE reflects bivariate enhancement effects.

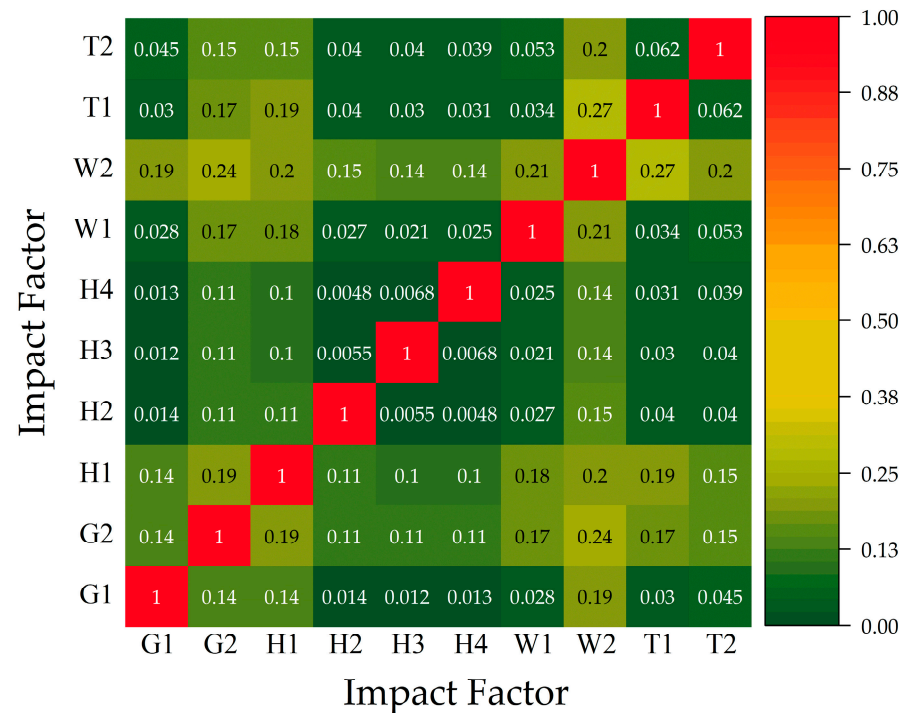


Figure 10. The result of factor interaction detection.

The ecological detection results of W2, G2, H1, and T2 are Y compared to most other impact factors, indicating significant differences and a high degree of independence among

them. Although these impact factors play a unique and significant role in the process of land subsidence, their mutual influence cannot be ignored.

There are 45 different forms of interaction between 10 impact factors, among which 82% of the factor combinations are nonlinear enhancement effects, and the remaining factor combinations are bivariate enhancement effects. The significant interaction between independent variables indicates that their influence on the independent variables is not independent. When there is interaction between independent variables, the explanatory power of the dependent variable is enhanced compared to independent effects, and the enhancement effect is manifested as a nonlinear enhancement or bivariate enhancement. A nonlinear enhancement refers to the effect of the interaction between two impact factors, resulting in explanatory power greater than the sum of explanatory power when acting alone. Although the strength of the bivariate enhancement is weak, its explanatory power still exceeds that of a single impact factor, indicating a complex interaction pattern between variables.

Even if the explanatory power of a single impact factor is weak, or the explanatory power of two impact factors is not strong enough, when they interact, the explanatory power of land subsidence will be significantly improved. Among them, the explanatory power of the interaction between the W2, T1, G2, and W1 of hydrological environment factors exceeds 20%, while the explanatory power of the interaction between H1 and T2, W1, and G2 exceeds 15%. This indicates that in the process of land subsidence, the interactions between these hydrological environmental factors are more significant and important than the effects of individual factors. Such interactions may involve multiple aspects, including changes in groundwater levels, interactions between surface water and groundwater, and the influence of geological structures on hydrological conditions. For example, changes in groundwater levels can affect the conditions for the replenishment and discharge of surface water, which, in turn, when combined with the geological background and topographical features, can lead to land subsidence. The decline in groundwater levels may cause the compression of underground aquifers, resulting in ground subsidence. At the same time, the interaction between surface water and groundwater, such as the replenishment or discharge of surface water, can also alter the flow paths and pressure distribution of groundwater, further affecting the spatial distribution and extent of land subsidence.

The interplay between geological background, hydrological environment, and topographic features is multifaceted, forming a complex system that collectively determines the patterns of ground subsidence. The dynamics of geological structures, including fault movements, folding, and magmatic activities, not only reshape the conditions for groundwater storage but also alter its recharge and flow paths. The movement of groundwater can dissolve minerals in rocks, altering the physical and chemical properties of the soil, and in certain cases, such as the erosive action of underground rivers, it can even change the morphology of the terrain. The undulations of the terrain affect not only the flow and distribution of surface water but also the recharge and drainage of groundwater. Therefore, the interactions among these factors play a crucial role in explaining the spatial and temporal variations of land subsidence, emphasizing the importance of considering the interactions of multiple factors in land subsidence research. Only by comprehensively considering the interactions of these factors can we more accurately understand and predict the dynamic trends of land subsidence.

4. Discussion

In this study, we calculated the rate of land subsidence of TSNSUA by utilizing Sentinel-1A SAR data, SRTM 30 m data, and other socio-economic data, and we analyzed the distribution patterns and impact factors.

This study employed the SBAS-InSAR technique for monitoring land subsidence. Compared to existing monitoring methods such as D-InSAR and PS-InSAR, SBAS-InSAR effectively overcomes the decorrelation issues caused by long spatial baselines, as well as the influence of terrain and atmospheric phases, by selecting multiple master images and appropriate spatiotemporal baseline thresholds. Additionally, this technique can monitor large areas of surface deformation and provide long time series of surface deformation data, making it suitable for regional geological disaster assessment and urban land subsidence monitoring. It also enables the analysis of trends in surface deformation. Through an in-depth analysis of land subsidence in the TSNSUA region, it is evident that subsidence is more severe in areas with active geological structures, excessive groundwater extraction, and dense human activities. Additionally, the presence of subsidence funnels causes land subsidence to exhibit a distinct clustering characteristic. Different cities experience varying processes and degrees of subsidence due to their unique topography, climate conditions, and urban development impacts. For instance, some cities may be more significantly affected by geological activities due to their undulating terrain, while others may face intensified subsidence due to insufficient groundwater replenishment caused by climatic conditions. The urbanization process, including changes in land use and infrastructure construction, also significantly impacts land subsidence. For example, large-scale urban development can lead to a decline in groundwater levels, thereby triggering subsidence. Therefore, it is crucial to develop targeted monitoring and management strategies based on the specific conditions of each city to effectively address land subsidence issues.

Through analyzing the factors affecting ground subsidence, we found that the hydrological environment has the greatest contribution to ground subsidence in TSNSUA. The region has a complex climate, including temperate continental and plateau mountain climates, with low and uneven annual precipitation, and most areas are in arid and semi-arid zones [47]. As urban development progresses, surface water is insufficient to meet the city's water demand, leading to overexploitation of groundwater. When groundwater is overexploited, the water table drops, disrupting the pressure balance between soil bodies, and the soil and rock bodies supported by groundwater are excessively compressed due to water loss, reducing in volume, forming funnel voids, and losing their load-bearing capacity for the ground. In addition, the pressure from surface buildings and transportation systems further compresses the soil or rock bodies, accelerating ground subsidence. Even if measures are later taken to raise the groundwater level, it is difficult for the soil or rock bodies to return to their original state, making ground subsidence irreversible [48].

The intricate geological backdrop significantly influences the occurrence of ground subsidence. TSNSUA, positioned at the forefront of the Tianshan Mountain range, is part of an active intracontinental orogen. Over the last 10 million years, this area has been subjected to vigorous tectonic movements and rapid erosional uplift, classifying it as a newly active tectonic zone. The subsidence in TSNSUA is predominantly found in regions rich in Quaternary unconsolidated sediments. Intense tectonic activities can reshape the landforms, affect the sediment distribution, alter the hydrological environment, and impact human activities, all of which can lead to ground subsidence. Earthquakes, a pronounced manifestation of geological tectonic activity, are indicative of the rapid release of stress within the crust. The earthquake data from the China Earthquake Networks Center (<https://news.ceic.ac.cn/>, accessed on 11 December 2023) reveal that between 2018 and 2022, TSNSUA was struck by 68 earthquakes of varying intensities. We extracted the surface subsidence rates at the epicenter (Figure 11) and found that most areas of the epicentral region experienced varying degrees of land subsidence. In the majority of these earthquake-prone areas, ground subsidence has been observed, highlighting the contribution of seismic activities and the subsequent subsidence they trigger to the overall

ground subsidence in the region. Expanding on this, the continuous tectonic uplift in the northern foothills of the Tianshan Mountains, with an uplift rate of approximately 1.2 to 4.8 mm per year since the last 13,000 years, suggests that the region is still undergoing active geological changes. These uplifts, combined with the spatial characteristics of ground subsidence across TSNSUA, indicate that different areas have experienced varying degrees of subsidence or uplift. The correlation between seismic activity and ground subsidence is further emphasized by the fact that areas prone to earthquakes have shown significant ground deformation, suggesting that the stress release during earthquakes not only causes immediate surface shaking but also leads to longer-term ground deformation and subsidence. This underscores the importance of considering tectonic and seismic activities when assessing and managing ground subsidence risks in TSNSUA and similar geologically active regions.

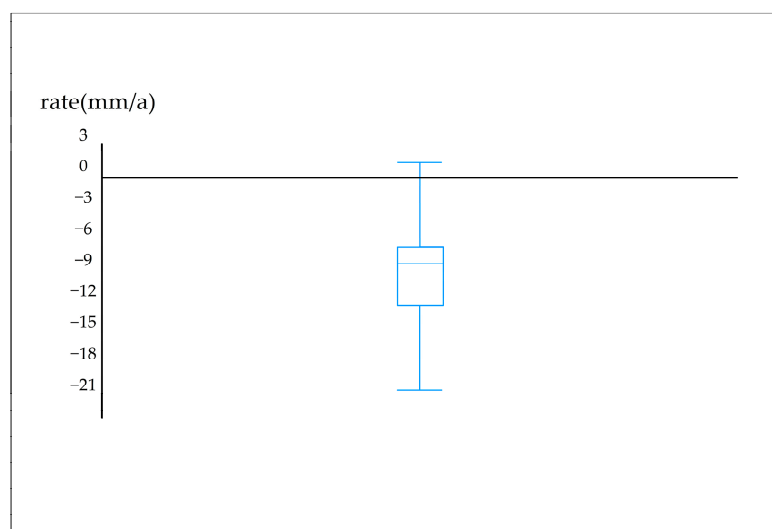


Figure 11. The box plot of epicenter deformation rates.

Additionally, TSNSUA is located on two key metallogenic belts, the Paleo Asian Ocean and the Tethys Ocean [49]. This region has undergone a long history of marine and terrestrial alternation, possessing a unique geological history and diverse mineralization processes. The widespread geological structures and relatively intact exposed strata provide excellent natural conditions for the enrichment and diversity of mineral resources, resulting in abundant and varied mineral reserves in the area.

During the initial stages of underground mining, excavation activities disrupt the original stress balance of the underground rocks. As mining progresses and subsurface mineral resources are extracted, voids are created, leading to displacement of the surrounding rocks and even broader areas of the rock mass. Over time, this results in ground subsidence. The extensive extraction of groundwater during mining operations causes surrounding groundwater to flow towards the mining area, disrupting the original stress balance of the groundwater and, thus, triggering widespread ground subsidence [50,51]. At the same time, mining activities often attract a large number of migrant workers, which may lead to a surge in demand for local housing, transportation, and public service facilities. This increases ground load and urban supply pressure, negatively impacting ground stability. Many mining areas within the TSNSUA region have experienced significant ground subsidence, such as in Changji City and Manas County, where some coal mining areas have shown particularly severe ground subsidence. Therefore, it can be concluded that the extraction of coal and other mineral resources is a significant cause of long-term, high-rate ground subsidence in certain areas of TSNSUA.

This study reveals that the influence of human activities on ground subsidence is relatively limited. On the one hand, the study predominantly attributes the changes in groundwater and mining activities to the effects of hydrological environments and tectonic movements, while considering a restricted range of human activity indicators, such as nighttime lighting and population density. On the other hand, TSNSUA, as one of China's 19 core urban agglomerations, has seen swift development due to the Western Development and Belt and Road Initiatives, yet it still lags behind the central and eastern regions in terms of the impact of human activities on ground subsidence. Nevertheless, urbanization and the surge of population are intensifying urban stressors, including excessive groundwater extraction and heightened ground loading, which could heighten the risk of ground subsidence—a factor that should not be disregarded [52].

In summary, the land subsidence phenomenon in TSNSUA is not directly caused by a single independent impact factor, but rather the result of multiple factors working together through complex interactions and mutually reinforcing effects. This multi-factor interaction leads to a comprehensive impact on the phenomenon of land subsidence, reflecting the complexity and diversity of the land subsidence process. And due to differences in regional characteristics, the ways and intensities of various factors also vary. Therefore, when studying and managing land subsidence issues, it is necessary to fully consider the regional characteristics and the interactions between various factors in order to develop targeted prevention and control measures to protect the geological environment and human living environment of the region.

This paper proposes a monitoring plan for ground subsidence in the TSNSUA area. To effectively manage and mitigate the impacts of ground subsidence, a comprehensive consideration of various factors such as geological structures, hydrological conditions, mineral resource extraction activities, and population growth is necessary. This includes implementing stricter groundwater management policies, optimizing methods of mineral resource extraction, strengthening infrastructure to accommodate increased loads, and planning urban development to minimize disruption to geological structures. Through these multifaceted measures, the geological environment can be better protected, ensuring sustainable development in the region. It is recommended that the government incorporate this monitoring plan into its existing planning tools. In the process, by providing valuable data support for geological disaster risk assessment and urban planning, establishing a ground subsidence monitoring and early warning system holds significant theoretical and practical importance for disaster prevention, mitigation, and safety monitoring. This contributes to enhancing the management level of urban geological environments and the capacity for risk prevention and disaster mitigation.

5. Conclusions

This study computed land subsidence within TSNSUA from 2018 to 2022 using Sentinel-1A SAR satellite images based on SBAS-InSAR technology. The spatiotemporal patterns of land subsidence and evolution trends were analyzed by using transition matrix and the landscape pattern index. The impact factor of land subsidence was developed based on 10 impact factors including geological background, human activities, hydrological environment, and terrain features, and we quantitatively analyzed the complex impact mechanism of land subsidence. The main conclusions are as follows:

- (1) The study used SBAS InSAR technology to obtain land subsidence information within TSNSUA from 2018 to 2022. The average land subsidence rate of TSNSUA is mainly distributed between -30 and 10 mm/a, and the maximum subsidence rate can reach -358 mm/a. Settlement mainly occurs in Hutubi County and Manas County.

- (2) The spatiotemporal distribution characteristics of land subsidence in TSNSUA from 2018 to 2022 were studied. The results indicate that in terms of spatial characteristics, the rate of land subsidence in the study area shows a clear spatial clustering distribution and exhibits positive spatial correlation, which is related to the formation of subsidence funnels in the subsiding areas. The pattern of land subsidence is primarily characterized by low subsidence rates and areas of uplift. Regarding temporal characteristics, during the monitoring period, each administrative district within the study area experienced varying degrees of subsidence and uplift.
- (3) The study used GeoDector software to quantitatively analyze the impact factors of land subsidence in TSNSUA and explored the impact mechanism of land subsidence in the study area. The quantitative results indicate that the hydrological environment is the primary factor influencing land subsidence, with a strong explanatory power and significant interactions with other factors. This is closely related to the arid and semi-arid climate conditions in the TSNSUA region, as well as the scarcity of groundwater resources.

In this study, we calculated the land subsidence rate and analyzed the spatiotemporal pattern and impact factor in TSNSUA. However, the shortcoming is that we did not analyze in depth the driving factors affecting the land subsidence, including groundwater and geological structures. Moreover, fewer reliability verification analyses were used in land subsidence, and more contemporaneous-level monitoring data or other measured data will be added in a later study for more scientific and accurate land subsidence.

Author Contributions: Conceptualization, H.C. and R.W.; methodology, X.Y., L.W. and H.C.; data curation, X.Y. and L.W.; writing—original draft preparation, X.Y., L.W. and H.C.; writing—review and editing, R.W. and H.Y.; visualization, X.Y.; resources, R.W., H.Y. and Z.Y. All authors have read and agreed to the published version of the manuscript.

Funding: This research was funded by the Third Xinjiang Scientific Expedition Program, grant number No.2022xjkk1006; the Xinjiang Uygur Autonomous Region Key Research and Development Program, grant number 2022B01012-1; the National Natural Science Foundation of China, grant number 52478011; the Science and Technology Innovation Project of Jiangsu Provincial Department of Natural Resources, grant number 2023018; the Open Research Project of The Hubei Key Laboratory of Intelligent Geo-Information Processing, grant number KLGIP-2023-A04.

Data Availability Statement: The data presented in this study are available upon request from the corresponding author. The data are not publicly available due to privacy.

Conflicts of Interest: The authors declare no conflicts of interest.

References

1. Ao, Z.; Hu, X.; Tao, S.; Hu, X.; Wang, G.; Li, M.; Wang, F.; Hu, L.; Liang, X.; Xiao, J.; et al. A national-scale assessment of land subsidence in China's major cities. *Science* **2024**, *384*, 301–306. [[CrossRef](#)]
2. Ouyang, L.; Zhao, Z.; Zhou, D.; Cao, J.; Qin, J.; Cao, Y.; He, Y. Study on the Relationship between Groundwater and Land Subsidence in Bangladesh Combining GRACE and InSAR. *Remote Sens.* **2024**, *16*, 3715. [[CrossRef](#)]
3. Bagheri-Gavkosh, M.; Hosseini, S.M.; Ataie-Ashtiani, B.; Sohani, Y.; Ebrahimian, H.; Morovat, F.; Ashrafi, S. Land subsidence: A global challenge. *Sci. Total Environ.* **2021**, *778*, 146193. [[CrossRef](#)]
4. Zhang, G.; Xu, Z.; Chen, Z.; Wang, S.; Liu, Y.; Gong, X. Analyzing surface deformation throughout China's territory using multi-temporal InSAR processing of Sentinel-1 radar data. *Remote Sens. Environ.* **2024**, *305*, 114105. [[CrossRef](#)]
5. Wei, Y.; Liu, X.; Zhao, C.; Tomás, R.; Jiang, Z. Observation of Surface Displacement Associated with Rapid Urbanization and Land Creation in Lanzhou, Loess Plateau of China with Sentinel-1 SAR Imagery. *Remote Sens.* **2021**, *13*, 3472. [[CrossRef](#)]
6. Sun, L.; Wang, X.; Wang, S.; Sun, W.; Wang, J.; Di, H. Experimental study on soil deformation caused by overexploitation of groundwater. *Water Environ. Res.* **2024**, *96*, e11111. [[CrossRef](#)]
7. Zhao, C.; Zhang, Q.; Yang, C.; Zhang, J.; Zhu, W.; Qu, F.; Liu, Y. Different scale land subsidence and ground fissure monitoring with multiple InSAR techniques over Fenwei basin, China. *Proc. Int. Assoc. Hydrol. Sci.* **2015**, *372*, 305–309. [[CrossRef](#)]

8. Jiang, Y.; Wang, J.; Yuan, X.; Wang, R. Analysis of the geomorphology and environmental geological problems of Huzhou on the Yangtze River delta. *Acta Geol. Sin. Engl. Ed.* **2004**, *78*, 808–812.
9. Zhang, Y.; Liu, Y.; Jin, M.; Jing, Y.; Liu, Y.; Liu, Y.; Sun, W.; Wei, J.; Chen, Y. Monitoring Land Subsidence in Wuhan City (China) using the SBAS-InSAR Method with Radarsat-2 Imagery Data. *Sensors* **2019**, *19*, 743. [[CrossRef](#)]
10. Li, D.; Li, B.; Zhang, Y.; Fan, C.; Xu, H.; Hou, X. Spatial and temporal characteristics analysis for land subsidence in Shanghai coastal reclamation area using PS-InSAR method. *Front. Mar. Sci.* **2022**, *9*, 1000523. [[CrossRef](#)]
11. Zhang, Z.; Hu, C.; Wu, Z.; Zhang, Z.; Yang, S.; Yang, W. Monitoring and analysis of ground subsidence in Shanghai based on PS-InSAR and SBAS-InSAR technologies. *Sci. Rep.* **2023**, *13*, 8031. [[CrossRef](#)]
12. Massonnet, D.; Rossi, M.; Carmona, C.; Adragna, F.; Peltzer, G.; Feigl, K.; Rabaute, T. The Displacement Field of the Landers Earthquake Mapped by Radar Interferometry. *Nature* **1993**, *364*, 138–142. [[CrossRef](#)]
13. Berardino, P.; Fornaro, G.; Lanari, R.; Sansosti, E. A new algorithm for surface deformation monitoring based on small baseline differential SAR interferograms. *IEEE Trans. Geosci. Remote Sens.* **2002**, *40*, 2375–2383. [[CrossRef](#)]
14. Ibrahim, H.B.; Salah, M.; Zazoura, F.; El-Mewafi, M. Differential synthetic aperture radar (SAR) interferometry for detection land subsidence in Derna City, Libya. *J. Appl. Geodesy* **2024**, *18*, 433–448. [[CrossRef](#)]
15. Wang, H.; Qi, Y.; Zhang, J.; Zhang, J.; Yang, R.; Guo, J.; Luo, D.; Wu, J.; Zhou, S. Influence of Open-Pit Coal Mining on Ground Surface Deformation of Permafrost in the Muli Region in the Qinghai-Tibet Plateau, China. *Remote Sens.* **2022**, *14*, 2352. [[CrossRef](#)]
16. Xue, Y.-A.; Zou, Y.-F.; Li, H.-Y.; Zhang, W.-Z. Regional subsidence monitoring and prediction along high-speed railways based on PS-InSAR and LSTM. *Sci. Rep.* **2024**, *14*, 24622. [[CrossRef](#)] [[PubMed](#)]
17. Hu, C.; Zhang, S.B.; Xu, S.Z.; Xu, B. Distributed Landslide Monitoring by Wireless Sensor Nodes. *Adv. Mater. Res.* **2012**, *594–597*, 1069–1073. [[CrossRef](#)]
18. Devaraj, S.; Yarrakula, K.; Martha, T.R.; Murugesan, G.P.; Vaka, D.S.; Surampudi, S.; Wadhwa, A.; Loganathan, P.; Budamala, V. Time series SAR interferometry approach for landslide identification in mountainous areas of Western Ghats, India. *J. Earth Syst. Sci.* **2022**, *131*, 133. [[CrossRef](#)]
19. Teixeira, A.C.; Bakon, M.; Perissin, D.; Sousa, J.J. InSAR Analysis of Partially Coherent Targets in a Subsidence Deformation: A Case Study of Maceió. *Remote Sens.* **2024**, *16*, 3806. [[CrossRef](#)]
20. Vaka, D.S.; Rao, Y.S.; Bhattacharya, A. Time series analysis of the pre-seismic and post-seismic surface deformation of the 2017 Iran–Iraq earthquake derived from Sentinel-1 InSAR data. *J. Earth Syst. Sci.* **2023**, *132*, 64. [[CrossRef](#)]
21. He, Y.; Qian, Z.; Chen, B.; Yang, W.; Hao, P. Surface Deformation of Xiamen, China Measured by Time-Series InSAR. *Sensors* **2024**, *24*, 5329. [[CrossRef](#)]
22. Zhang, P.; Qian, X.; Guo, S.; Wang, B.; Xia, J.; Zheng, X. A New Method for Continuous Track Monitoring in Regions of Differential Land Subsidence Rate Using the Integration of PS-InSAR and SBAS-InSAR. *Remote Sens.* **2023**, *15*, 3298. [[CrossRef](#)]
23. Yang, Z.F.; Li, Z.W.; Zhu, J.J.; Preusse, A.; Yi, H.W.; Wang, Y.J.; Papst, M. An Extension of the InSAR-Based Probability Integral Method and Its Application for Predicting 3-D Mining-Induced Displacements Under Different Extraction Conditions. *IEEE Trans. Geosci. Remote Sens.* **2017**, *55*, 3835–3845. [[CrossRef](#)]
24. Hu, J.; Li, Z.; Ding, X.; Zhu, J.; Zhang, L.; Sun, Q. Resolving three-dimensional surface displacements from InSAR measurements: A review. *Earth-Science Rev.* **2014**, *133*, 1–17. [[CrossRef](#)]
25. Ahmed, G.; Zan, M.; Helili, P.; Kasimu, A. Responses of Vegetation Phenology to Urbanisation and Natural Factors along an Urban-Rural Gradient: A Case Study of an Urban Agglomeration on the Northern Slope of the Tianshan Mountains. *Land* **2023**, *12*, 1108. [[CrossRef](#)]
26. Zhang, J.; Kou, P.; Tao, Y.; Jin, Z.; Huang, Y.; Cui, J.; Liang, W.; Liu, R. Urban ground subsidence monitoring and prediction using time-series InSAR and machine learning approaches: A case study of Tianjin, China. *Environ. Earth Sci.* **2024**, *83*, 473. [[CrossRef](#)]
27. Wen, Q.; Zhao, X.; Zhang, Z.; Wang, C.; Zeng, T.; Zhang, M. Spatial structures of Chinese Urban Agglomerations in the “Silk Road Economic Belt”. In Proceedings of the 2018 Fifth International Workshop on Earth Observation and Remote Sensing Applications (Eors), Xi’an, China, 18–20 June 2018; pp. 356–360.
28. Lee, J.; Yin, X.; Zhu, H. Spatial Optimization of Land Use Allocation Based on the Trade-off of Carbon Mitigation and Economic Benefits: A Study in Tianshan North Slope Urban Agglomeration. *Land* **2024**, *13*, 892. [[CrossRef](#)]
29. Zhao, Y.; Kasimu, A.; Gao, P.; Liang, H. Spatiotemporal Changes in The Urban Landscape Pattern and Driving Forces of LUCC Characteristics in The Urban Agglomeration on The Northern Slope of The Tianshan Mountains from 1995 to 2018. *Land* **2022**, *11*, 1745. [[CrossRef](#)]
30. Guo, J.; Hu, J.; Li, B.; Zhou, L.; Wang, W. Land subsidence in Tianjin for 2015 to 2016 revealed by the analysis of Sentinel-1A with SBAS-InSAR. *J. Appl. Remote Sens.* **2017**, *11*, 026024. [[CrossRef](#)]
31. Ashraf, T.; Yin, F.; Liu, L.; Zhang, Q. Land Subsidence Detection Using SBAS- and Stacking-InSAR with Zonal Statistics and Topographic Correlations in Lakhra Coal Mines, Pakistan. *Remote Sens.* **2024**, *16*, 3815. [[CrossRef](#)]
32. Guo, H.; Martínez-Graña, A.M. Susceptibility of Landslide Debris Flow in Yanghe Township Based on Multi-Source Remote Sensing Information Extraction Technology (Sichuan, China). *Land* **2024**, *13*, 206. [[CrossRef](#)]

33. Yan, L.; Xiong, Q.; Li, D.; Cheon, E.; She, X.; Yang, S. InSAR-Driven Dynamic Landslide Hazard Mapping in Highly Vegetated Area. *Remote Sens.* **2024**, *16*, 3229. [[CrossRef](#)]
34. Wang, Z.; Liu, Y.; Zhang, Y.; Liu, Y.; Wang, B.; Zhang, G. Spatially Varying Relationships between Land Subsidence and Urbanization: A Case Study in Wuhan, China. *Remote Sens.* **2022**, *14*, 291. [[CrossRef](#)]
35. Marcińczak, S.; Iglesias-Pascual, R.; Kopeć, D.; Wróbel, K.; Mooses, V. Landscapes of thermal inequality: Exploring patterns of climate justice across multiple spatial scales in Spain. *Landsc. Urban Plan.* **2024**, *254*, 105255. [[CrossRef](#)]
36. Wang, J.; Xu, C. Geodetector: Principle and prospective. *Acta Geogr. Sin.* **2017**, *72*, 116–134.
37. Wang, R.; Wang, M.; Zhang, Z.; Hu, T.; Xing, J.; He, Z.; Liu, X. Geographical Detection of Urban Thermal Environment Based on the Local Climate Zones: A Case Study in Wuhan, China. *Remote Sens.* **2022**, *14*, 1067. [[CrossRef](#)]
38. Wu, K.; Su, W.; Ye, S.; Li, W.; Cao, Y.; Jia, Z. Analysis on the geographical pattern and driving force of traditional villages based on GIS and Geodetector: A case study of Guizhou, China. *Sci. Rep.* **2023**, *13*, 20659. [[CrossRef](#)]
39. Duan, Y.; Gao, Y.G.; Zhang, Y.; Li, H.; Li, Z.; Zhou, Z.; Tian, G.; Lei, Y. “The 20 July 2021 Major Flood Event” in Greater Zhengzhou, China: A Case Study of Flooding Severity and Landscape Characteristics. *Land* **2022**, *11*, 1921. [[CrossRef](#)]
40. Ouyang, Y.; Feng, T.; Feng, H.; Wang, X.; Zhang, H.; Zhou, X. Deformation Monitoring and Potential Risk Detection of In-Construction Dams Utilizing SBAS-InSAR Technology—A Case Study on the Datengxia Water Conservancy Hub. *Water* **2024**, *16*, 1025. [[CrossRef](#)]
41. Ren, K.; Li, R.; Yao, X.; Zhao, X.; Ma, L.; Yao, C.; Jiang, S.; Gu, Z.; Zhou, Z. Monitoring Yanwan deep-seated toppling deformation with the impact of water-level fluctuation by SAR observations. *Landslides* **2024**, *21*, 1243–1254. [[CrossRef](#)]
42. Jasechko, S.; Seybold, H.; Perrone, D.; Fan, Y.; Shamsudduha, M.; Taylor, R.G.; Fallatah, O.; Kirchner, J.W. Rapid groundwater decline and some cases of recovery in aquifers globally. *Nature* **2024**, *625*, 715–721. [[CrossRef](#)] [[PubMed](#)]
43. Zhang, N.; Liu, X.; Zhang, Y.; Gu, H.; Yan, B.; Jia, Q.; Gao, X. Investigating the Mechanism of Land Subsidence Due to Water Network Integration at the Guangzhou Longgui Salt Mine and Its Impact on Adjacent Subway. *Water* **2024**, *16*, 1723. [[CrossRef](#)]
44. Zhao, X.; Chen, B.; Gong, H.; Zhou, C.; Li, X.; Lei, K.; Ke, Y. Land subsidence along the Beijing-Tianjin Intercity Railway during the period of the South-to-North Water Diversion Project. *Int. J. Remote Sens.* **2020**, *41*, 4447–4469. [[CrossRef](#)]
45. Zhang, Y.; Jiang, Z.; Cheng, X. Differential sar interferometry for mining subsidence detection in rugged terrain. In Proceedings of the IGARSS 2011—2011 IEEE International Geoscience and Remote Sensing Symposium, Vancouver, BC, Canada, 24–29 July 2011; pp. 2204–2207.
46. Zhang, J.-Z.; Huang, H.-J.; Bi, H.-B. Land subsidence in the modern Yellow River Delta based on InSAR time series analysis. *Nat. Hazards* **2015**, *75*, 2385–2397. [[CrossRef](#)]
47. Chen, Z.; Li, Z.; Xu, L.; Zhou, X.; Zhang, X.; Wang, F.; Luo, Y. Gaseous and Particulate Pollution in the Wu-Chang-Shi Urban Agglomeration on the Northern Slope of Tianshan Mountains from 2017 to 2021. *Atmosphere* **2023**, *14*, 91. [[CrossRef](#)]
48. Qin, M.; Yang, J.; Bai, Y.; Bai, Y. The subsidence–distance relationship for land subsidence induced by groundwater abstraction. *Hydrogeol. J.* **2024**, *32*, 1–13. [[CrossRef](#)]
49. Hu, L.; Du, Y.; Xu, Y.; Wang, Z.; Wang, C. New Zircon U-Pb Age of Late Devonian Tuff in Guangxi, South China and the Significance for the Paleo-Tethys Branch Ocean. *Acta Geol. Sin. Engl. Ed.* **2018**, *92*, 402–403. [[CrossRef](#)]
50. Du, Z.; Feng, L.; Wang, H.; Dong, Y.; Luo, D.; Zhang, X.; Liu, H.; Zhang, M. Identification of Ground Deformation Patterns in Coal Mining Areas via Rapid Topographical Analysis. *Land* **2023**, *12*, 1221. [[CrossRef](#)]
51. Tan, H.; Yu, X.; Zhu, M.; Guo, Z.; Chen, H. Deformation Monitoring and Spatiotemporal Evolution of Mining Area with Unmanned Aerial Vehicle and D-InSAR Technology. *Mob. Inf. Syst.* **2022**, *2022*, 8075611. [[CrossRef](#)]
52. Tang, W.; Ng, A.H.-M.; Wang, H.; Kuang, J.; Du, Z. Surface Subsidence Characteristics and Causes Analysis in Ningbo Plain by Sentinel-1A TS-InSAR. *Remote Sens.* **2024**, *16*, 2438. [[CrossRef](#)]

Disclaimer/Publisher’s Note: The statements, opinions and data contained in all publications are solely those of the individual author(s) and contributor(s) and not of MDPI and/or the editor(s). MDPI and/or the editor(s) disclaim responsibility for any injury to people or property resulting from any ideas, methods, instructions or products referred to in the content.